AUTOMATIC GAIN CONTROL NETWORKS FOR MULTIDIMENTIONAL VISUAL ADAPTATION

S. Furman and Y. Y. Zeevi
Faculty of Electrical Engineering, Technion, Haifa 32000, Israel

Keywords: Non-linear Recurrent NN, Visual Adaptation, AGC, HVS, Size, Depth, Curvature, Enhancement.

Abstract: Processing and analysis of images are implemented in the multidimensional space of visual information representation. This space includes the well investigated dimensions of intensity, color and spatio-temporal frequency. There are, however, additional less investigated dimensions such as curvature, size and depth (for example - from binocular disparity). Along these dimensions, the human visual system (HVS) enhances and emphasizes important image attributes by adaptation and nonlinear filtering. It is interesting and possible to emulate the visual system processing of images along these dimensions, in order to achieve intelligent image processing and computer vision. Sparsely connected, recurrent adaptive sensory neural network (NN), incorporating non-linear interactions in the feedback loops, are presented. Such generic NN exhibit Automatic Gain Control (AGC) model of processing along the visual dimensions. The results are compared with those of psychophysical experiments exhibiting good reproduction of visual illusions.

1 INTRODUCTION

The perceived image is quite different from the original image projected onto the retina. Some of the image features are enhanced, while others are being adapted to or even ignored. Some features are of great importance, while other are barely noticed.

Understanding the organization and functioning of visual systems is obviously of great interest and importance to brain scientists and engineers because of its potential use in the design of technological systems. By matching image presentations (or storage) with the known performance of the visual system, more meaningful and efficient communication can be achieved. After all, most information generated for human use, is communicated with the human observer via the visual system as the final receiver. In yet another way, image processing modelled after the visual system may prove to be important in machine vision. And of course, if visual prosthetics are to become a workable reality, this understanding is essential.

Each cone in the central fovea is connected to about 4000 cortical neurons (Zeevi & Kronauer 1985). The challenge is to determine what the 4000 or so different processes are, and then how they are ordered in the tissue volume. Orientation and ocular dominance (OD) (Hubel & Wiesel 1979) can account for 40 different processing units (20 different orientations for each ocular projection). This leaves an unexplained factor of 4000/40=100! There are several candidates for the remaining functions, such as color, intensity, texture, curvature, range of field sizes and binocular disparity (for depth perception).

Gibson (1937) had claimed that adaptation and negative after-effect are to be conceived as a process of adjustment and readjustment of the physical-phenomenal correspondence of a certain type of sensory dimension, under the influence of a tendency for sensory activity to become normal, standard or neutral. He noticed that this similarity cuts across the sensory modalities of our world, including pressure, size, distance, temperature, brightness, curvature (convex-concave), etc.

Zeevi & Mangoubi (1978) showed that Adaptation plays an important role in the suppression of quantal and receptor internal noise. Wainwright (1999) proposed that visual adaptation in orientation, spatial frequency, and motion can be understood from the perspective of optimal information transmission.

Automatic Gain Control (AGC) has been widely used to account for intensity adaptation (Shefer 1979) contrast adaptation in the primary visual

Furman S. and Zeevi Y..
AUTOMATIC GAIN CONTROL NETWORKS FOR MULTIDIMENTIONAL VISUAL ADAPTATION.
DOI: 10.5220/0003061901630175
In *Proceedings of the International Conference on Fuzzy Computation and 2nd International Conference on Neural Computation* (ICNC-2010), pages 163-175
ISBN: 978-989-8425-32-4

cortex (Weltsch-Cohen 2002), contrast adaptation for "cyclopean" image (Ding & G. Sperling 2006), contrast adaptation for motion detection (Lu & George Sperling 1996) chromatic adaptation (Du Croz & Rushton 1966) and (Krauskopf & Mollon 1971), and sound adaptation (Schwartz & Simoncelli 2001). It is, therefore, natural and tempting to implement AGC NN which incorporates some other, less investigated dimensions of adaptation, such as size, depth and curvature in processing of images. Likewise, such an investigation may facilitate our understanding of how adaptation along these dimensions takes place in the visual system (or other sensory modalities for this matter).

The purpose of this study is to analyze adaptation along these image dimensions and process these image attributes by means of the AGC model in order to mimic the human visual system (HVS), and to propose a unified model for biological sensory processing. Likewise, the AGC mechanism considered in the context of visual systems (biological and ANN-based alike), can be also implemented in advanced image processing algorithms that highlight various image structures and feature. The performance of the proposed AGC NN is tested by computer simulations, using Matlab, for each dimension separately.

2 VISUAL AGC MODEL

The proposed AGC model of visual adaptation is based on the original work of Shefer (1979), and on the subsequent development of the adaptive sensitivity camera that mimics the eye (Ginosar et al. 1992) and (Zeevi et al. 1995). The model has been motivated by the structure and function of the eye and, in particular, by its high spatio-temporal sensitivity to small changes in intensity accomplished over extremely wide dynamic range. According to this nonlinear adaptation model, the output of a cell in location "i" is adjusted by subtracting from its input a nonlinear function of its input and a weighted sum of the outputs, fed back into the nonlinear synaptic operator (Fig. 1):

$$r_i = \alpha \cdot s_i - \mathcal{T}(s_i, f_i)\,, \qquad (1)$$

where r_i is the output, s_i is the input, W is a feedback operator (matrix), f_i is the feedback (see Eq. 2), α is a constant and $\mathcal{T}$ is a nonlinear function. The crucial ingredient of this AGC model is the nonlinearity within the feedback loop (i.e. the function $\mathcal{T}$). This is a fundamental extension of the lateral inhibition recurrent NN into the nonlinear regime, presumed to be mediated biologically by the retinal interplexiform cells and/or similar structures in other sensory neural networks, such as the synaptic depression (Abbott et al. 1997). It is important to note that qualitatively $\mathcal{T}$ may assume a wide range of nonlinear functions and, yet, the neural feedback loop in which such nonlinear synaptic interactions are embedded will exhibit functional AGC.

In a specific embodiment of this general conceptual model, the nonlinearly component is a multiplier (Fig. 2a). The model is then comprised of a series of static multipliers, one for each foveal receptor channel that multiply the input of the channel with the output of the feedback. The feedback is calculated by subtracting the output of the operator "W" from a constant value. The operator "W" is an averaging operator (in space).

The analytic domain of the model, in which we will be interested, is the upper right handed quarter of the multiplier. It is possible to choose the operator "W" so the model will operate at the analytic domain for an input i changing in a defined known range. We will assume that this is the case.

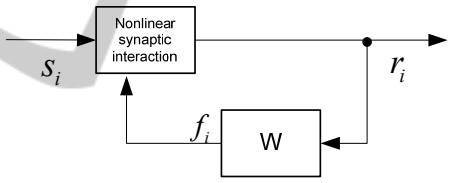

Figure 1: AGC model.

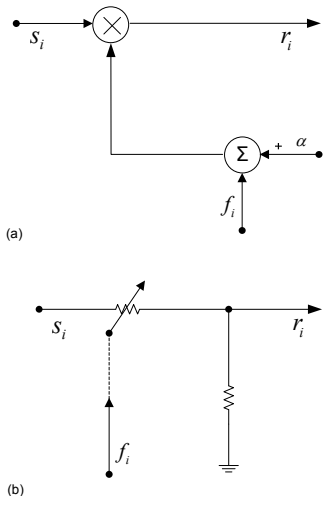

Figure 2: Gain control device. (a) Schematic drawing; (b) Hypothetic explicit implementation.

The presented AGC NN necessitates the existence of

controlled gain device. One option for such a device is shown in Fig. 2b. Bruckstein and Zeevi (1979) showed that the gain control of Fig. 2 can be implemented by a neural coding scheme with threshold control.

Each of the functions of the model is of an image dimension (curvature, size and depth). The feedback is obtained by:

$$f_i = \sum_j w_{ji} r_j \ . \tag{2}$$

Therefore the AGC model output is given by:

$$r_i = s_i(\alpha - \sum_j w_{ji} r_j) \ . \tag{3}$$

The function of the feedback is to position symmetrically the oparting curve around the operating point. W can be chosen as exponent, gaussian, triangle, rectangular or any other symmetric kernel without effect on the main characters of the model.

The model has a unique solution for

$$s_i \geq 0 \ \forall i \quad and \quad \max_i \{s_i\} < 1/S_W \ , \tag{4}$$

where S_W is:

$$S_W = \sum_j w_{ji} \ . \tag{5}$$

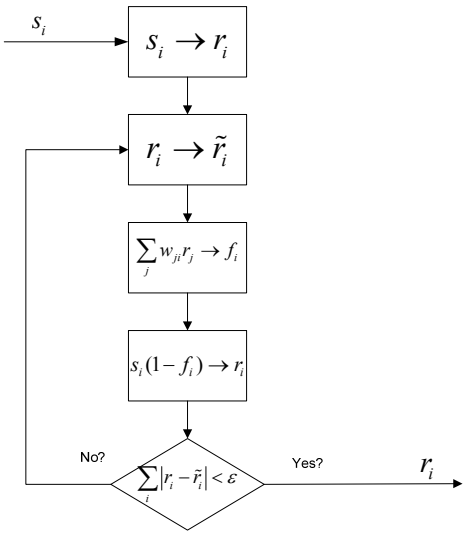

Figure 3: Flow chart for calcuating the visual AGC response to some arbitrary input.

2.1 Small Signal Analysis

Although we are concerned with "large signal" behaviour of the visual AGC, it is still useful to perform small signal analysis of the model. For that we assume that both the output and the input of the model are composed of a 'local DC', C_s (where local is defined on the scale of effective W) modulated by a small AC signal component:

$$S_i = C_s + s_i \ , \tag{6}$$

$$\sum_i s_i = 0 \ , \tag{7}$$

$$R_i = C_r + r_i \ , \tag{8}$$

$$\sum_i r_i = 0 \ . \tag{9}$$

For simplicity, we assume also that W is a rectangular function. Under these assumptions, (2) yields:

$$f_i = \sum_j w_{ji} R_j = C_r \ , \tag{10}$$

substituting (6),(7),(8),(9) and (10) in (3), we get:

$$r_i = s_i \frac{\alpha}{1+C_s} \ ; C_r = \frac{\alpha \cdot C_s}{1+C_s} \ . \tag{11}$$

Equation (11) expresses a sigmoidal function, which is closely related to Weber law. The latter implies that the system gain is inversely proportional to the input's average.

Weber law is characteristic for many sensory modalities, including weight, vision and sound.

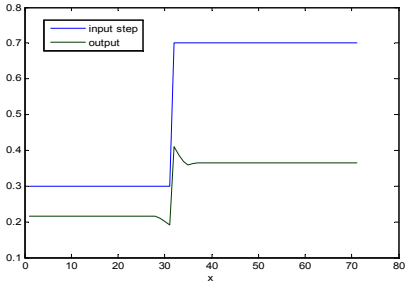

Figure 4: AGC model step response.

2.2 Simulation Method

In its discrete form, Eq. (3) exhibits the complexity of a manybody problem. To obtain a closed form solution for some arbitrary input is a major challenge, not yet dealt with. Therefore, we use a numeric solution of an iterative process. In the discrete final case, the solution is unique if the process converges (Shefer 1979). Fig. 3 presents the flow chart of the algorithm for numeric solution of the AGC model.

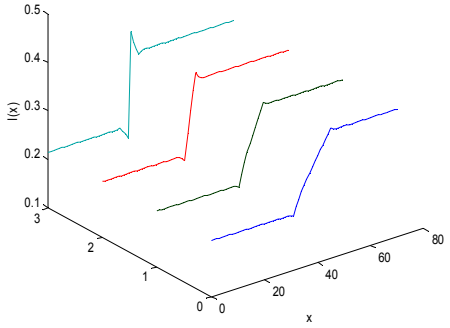

Figure 5: Ramp responses for various input slopes.

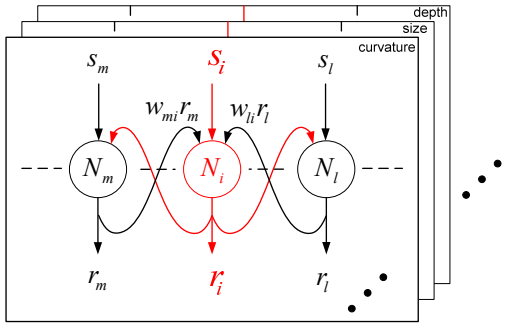

Figure 6: AGC NN.

2.3 Step Response for AGC Model

Fig. 4 depicts step response of the non-linear AGC model, superimposed on the step. This example highlights the main characteristics of the model:

- The adapted response to a locally-constant input is being decreased, while high values are more affected than lower values. This is, in a way, compression of a wide dynamic range of the input.
- An edge enhancement – the relative contrast is increased. This is caused by the overshoot and undershoot of the model response. Note that due to the nonlinearity of the model, the overshoot is stronger than the undershoot. Fig. 5 shows another nonlinear effect – the overshoot/undershoot are depended on the slop of the input step. The response is stronger for steeper slopes. When the input represents intensity, this phenomenon is the well known "Mach Bands" (Ratliff 1965).

2.4 AGC NN

The adaptive, non-linear, recurrent NN which exhibits multidimensional AGC characteristics constitutes in its functional complexity a case of a many-body problem. Yet, due to the local characteristics of W in the case of visual information processing, the network is sparsely connected and the implementation is simple and efficient with only one layer of a recurrent neural network (RNN). Fig. 6 depicts a schematic structure of such a RNN. One should keep in mind that each neuron represents a nonlinear function, as shown in Fig. 7. This is biologically feasible (as discussed above). It can be implemented in NN by other types of nonlinearities and architechtural embodiments.

3 BACKGROUND

3.1 Localness and Parallelism

A key fact regarding the structural-functional organization of the HVS (which support our AGC NN model) is that processing along the image dimensions of size, curvature, depth and/or other dimensions is performed locally and in parallel over the entire image (Hochstein & Ahissar 2002). These image dimensions are believed to be part of the "Elementary Features" (Cavanagh et al. 1990), (Wolfe et al. 2003) of the image representation in the HVS. In this case, the image is decomposed along a number of dimensions and into a number of separable components, and some specific cells represent that local information (a concept introduced by Hubel and Wiesel (1968) within the context of retinotopic representation).

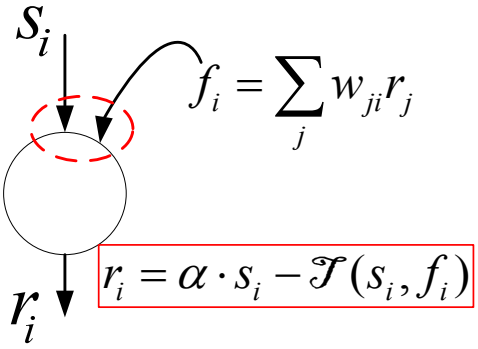

Figure 7: Nonlinear function of each neuron.

This concept had been tested in many psychophysical experiments such as “pop-ups”. In these experiments, there is a target with a unique feature which is not shared by the distractors.
If the feature is coded early in the visual processing and is performed locally and in parallel, the target

tends to “pop-up” from the distractors with little effect of the number of distractors. The features may either be discrete and categorical elements (e.g., terminators) that can be only present or absent, or they may be values on a continuous dimension that activate nonoverlapping populations of functional detectors and that, therefore, also mediate categorical discriminations. Treisman & Gormican (1988) showed that such "pop-up"s are asymmetric in that some features are detected more easily when they are present rather than when they are absent. Fig. 8 (adopted form (Treisman & Gormican 1988)) presents an example of such experiment for a target defined by curvature, while Fig. 9 presents an example of such experiment for target defined by depth cues (See Enns & Rensink (1990a), (1990b)).

Thus, we may conclude that size, curvature and depth are processed locally and in parallel.

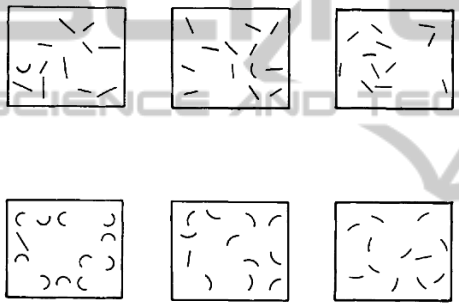

Figure 8: Examples of displays testing search for targets defined by curvature or ‘straightness’.

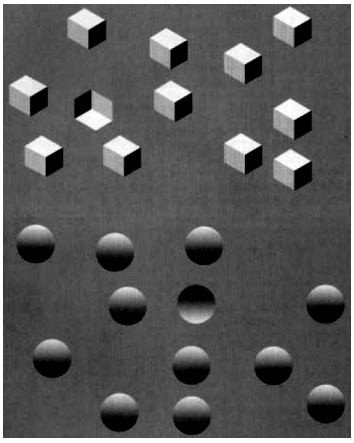

Figure 9: Two examples of display, testing search for targets defined by depth cues.

3.2 Adaptation and Feature Detectors

It is well known that prolonged inspection of a curved line causes adaptation to curvature (e.g. the curvature after-effect (Gibson 1937) and (Coltheart 1971)). Such after-effects are believed to reflect a change in the sensitivity of neurons that encode the adapted feature and, thus, imply the existence of neurons that act as detectors of that feature (Hancock & Peirce 2008).

Indeed, most of the investigators agree that curvature detectors are present along the early stages of the visual pathway (Riggs 1973), (Stromeyer & Riggs 1974). Some investigators even showed how such curvature calculations can be achieved by convolution with certain reasonable receptive fields of neural cells (Koenderink & Doorn 1987), (Dobbins et al. 1987).

Sutherland (1968) concluded that many species have the capacity to classify a shape as the same shape regardless of changes in size, at least over a considerable range, and that this capacity is innate. This ability can be addressed as irrelevance of the DC component of the size information (adaptation) and relevance of changes only.

Blakemore and Campbell (1969) suggested that the human visual system may possess neurons selectively sensitive to size. They also suggested that this neural system may play an essential preliminary role in the recognition of complex images. Carey et al (1996) suggested that size, motion and orientation measures are processed in parallel by the dorsal stream mechanisms.

The visual system perceives depth based on several cues such as stereoscopic views, motion-parallax, object size, object translation and rotation (Bruno & Cutting 1988), (Dijkstra et al. 1995), (Rogers & Graham 1979), (Bradshaw & Rogers 1996) and (Bradshaw et al. 2000). Hubel and Wiesel (1962), (1970) have identified the cells that are involved in depth information representation from stereoscopic vision (“complex cells”). Inui et al (2000) have discovered that an area involved in monocular depth processing in the bilateral occipitotemporal region.

It, therefore, seems reasonable to assume that curvature, size and depth information are calculated over the entire image (in parallel), wherein each of the cells contains the feature information of a specific location - each cell represents the feature information of a specific part of the image and together they create a projection of the image into a specific image dimension, where the location of the cells matches the location of the feature in the image. Based on this reasoning, it is natural to use AGC NN in processing of these image dimensions in vision.

3.3 Overview of Differential Geometry

It is useful to review a few elementary notions of differential geometry to establish the context in which the curvature processing is formulated. The review is focused on curves in the plane, although generalizations to higher dimensional curves exist.

Let I be an interval in one-dimensional Euclidian space E^1. A curve C is defined as a continuous mapping $x: I \to E^2$ from the interval to the plane where

$$x(\lambda) = (x_1(\lambda), x_2(\lambda)), \tag{12}$$

with $\lambda \in I$ being a parameter running along the curve, and x_1, x_2 are continuous functions of λ. The curve is said to have order of continuity k, denoted by C^k, where all derivatives up to and including the k[th] derivative of x_1 and x_2 are continuous. A curve may be reparameterized in terms of its arc length s, equivalent to a particle travelling at constant unit velocity along the curve. In this case, the tangent vectors are unit length vectors:

$$x'(s) = t(s) = (x_1'(s), x_2'(s)), \tag{13}$$

where $s = f(\lambda)$ is a reparameterization of the curve, and $\|x'\| = 1$. The interesting aspect of the tangent is its orientation. The geometric interpretation of the tangent to a curve is depicted in Fig. 10(a). Letting P be a point on a curve, and A a neighboring point, the tangent T at P is the limit of the line AP as A approaches P along the curve. The tangent yields the orientation of a curve at a point. Taking the second derivative with respect to s everywhere along C, we obtain

$$x''(s) = (x_1''(s), x_2''(s)), \tag{14}$$

where the vector $x''(s)$ is normal to the vector $x'(s)$ and the magnitude of $x''(s)$ is the curvature of C:

$$\kappa = \|x''(s)\| = \sqrt{x_1''^2(s) + x_2''^2(s)}. \tag{15}$$

Curvature is a measure of the rate of change of orientation per unit arc length. The geometric interpretation for the curvature is depicted in Fig. 10(b). Let P be a point on a curve, T the tangent at that point, and A a neighboring point on the curve.

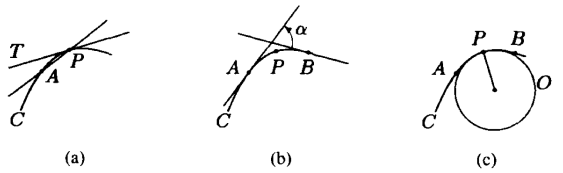

Figure 10: (a) Tangent T is the limit of segment PA as A approaches P along C. (b) The curvature κ of C at P is the limit of the ratio α /AB as A and B approach P independently along C. (c) The osculating circle 0 at P is the limit of the circle that passes through A, P, and B, as A and B approach P.

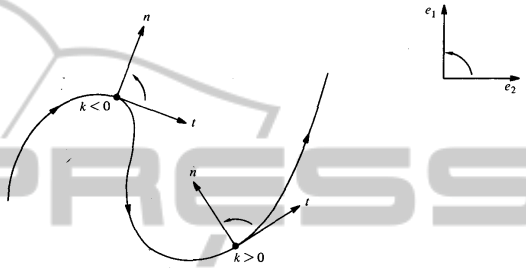

Figure 11: Signed curvature.

Let α denote the angle between the line AP and T, and AB the arc length between A and B. The curvature κ at P is the limit of the ratio α /AB as A approaches P along the curve. Related to this interpretation of curvature is the osculating circle. Referring to Fig. 10(c), let A, P, and B be three neighboring points on a curve, and let U be a circle through these points. As A and B independently approach P along the curve, the circle O converges towards a limit, whose radius is precisely the inverse of the curvature κ at P.

$$R = \frac{1}{\kappa}. \tag{16}$$

Since the curve is a plane curve (that is, $x(I)$ is contained in a plane), it is possible to associate a sign with the curvature κ. To this end, let $\{e_1, e_2\}$ be the natural basis of R^2, and define the normal vector $n(s), s \in I$, by requiring the basis and might be either positive or negative. It is clear that $|\kappa|$ agrees with the previous definition and that κ changes sign when we change either the orientation of x or the orientation of R^2 (see Fig. 11). In this work, we use the signed curvature notation. The signed curvature indicates the direction along which the unit tangent vector rotates as a function of the parameter along the curve.

$\{t(s), n(s)\}$ to have the same orientation as the basis $\{e_1, e_2\}$. The signed curvature κ is then defined (instead of (15)) by

$$t'(s) = \kappa n, \quad (17)$$

If the unit tangent rotates counter clockwise, then $\kappa > 0$. If it rotates clockwise, then $\kappa < 0$.

The signed curvature depends on the particular parameterization chosen for a curve.

4 PSYCHOPHYSICAL EXPERIMENTS

For illustrative purpose, two psychophysical experiments are presented as an example. The first is for size contrast effect (the Ebbinghaus illusion). The second is for depth contrast effect. The AGC model reproduces the illusions.

4.1 Size Contrast

The Ebbinghaus illusion is commonly used as an example of a simple size-contrast effect. In this illusion, the apparent size of a central target is changed by a ring of surrounding inducers. Fig. 12 illustrates its most popular form, as it most often appears in general textbooks. In this form, it is typically used to illustrate a simple size-contrast effect, in which large inducers make the target appear smaller whilst small inducers make it appear larger.

Roberts et al (2005) have further investigated the above effect and concluded that it probably arises from a number of factors that are:

- The relative size and number of the inducers (comparing to the target): For a given distance between the target and the inducers, the magnitude of the Ebbinghaus illusion is governed by the relative size and number of the inducers
- The distance between the central target and the inducers: For a given number and size of inducers, the magnitude of the Ebbinghaus illusion is governed by the distance between the central target and the inducers.
- The completeness of the inducing annulus: Keeping the number of the inducers constant, and changing their size (or distant), provides a change in the completeness of the inducing annulus. This confounding effect can be removed (the inducing annulus can be kept constant) by changing also the number of the inducers.

The authors performed several experiments, and the main findings were:

4.1.1 Experiment 1

Varying the relative size of the inducers in the Ebbinghaus illusion produces changes in the apparent size of the target, consistent with a size-contrast effect. Increasing inducer distance causes a decrease in apparent target size irrespective of inducer size. [Distance is measured from the centre of the target to the centre of the inducers.]

Fig. 13 shows, separately for each inducer distance, the average illusion magnitude, as a function of inducer radius. Based on these results, the authors concluded that "inducers generally reduce apparent target size and that small inducers are simply less effectual in doing this", and that "Inducer distance also has an effect, so that the reduction in target size tends to be more pronounced at greater distances".

To summarize, the apparent size of the target is reduced more efficiently when the inducers get bigger and at greater distances.

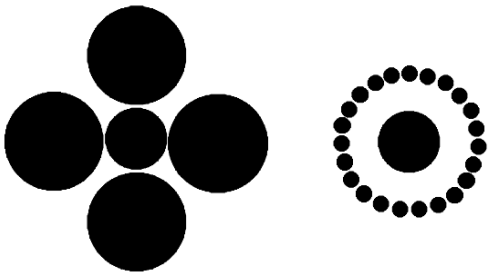

Figure 12: The Ebbinghaus illusion.

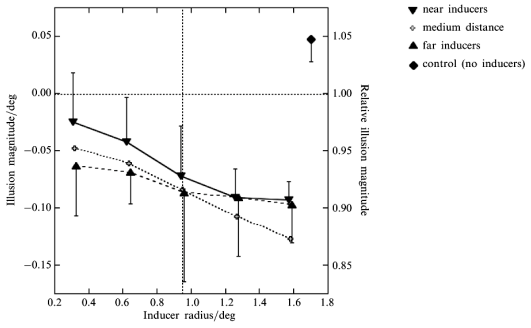

Figure 13: Results of experiment 1 from (Roberts et al. 2005).

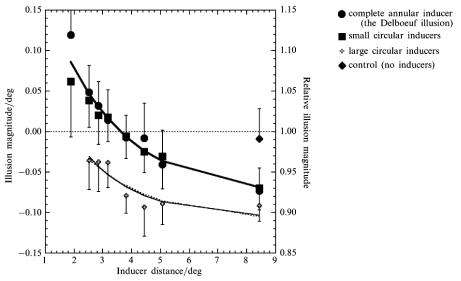

Figure 14: Results of experiment 3 from (Roberts et al. 2005).

4.1.2 Experiment 3

Here, The authors kept the inducing annulus and inducer size constant and study the effect of inducer distance. The results are given in Fig. 14. The authors conclude that the data can be modelled by the equation $a + b\exp(-x/c)$ and that the effect is governed mainly by two terms – inducers distance from the target (which described by decaying exponential), and by the inducers size which modulate this function.

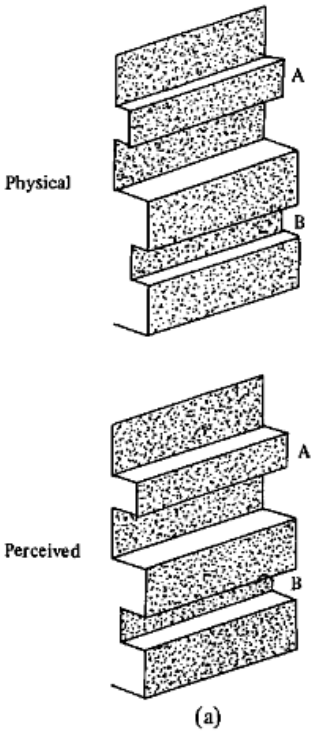

Figure 15: Bar A appeared to lie in front of bar B, although are physically at the same depth.

4.2 Depth Contrast

Graham and Rogers (1982) have shown depth-contrast effect perceived from motion parallax and stereoscopic information. Their results are shown in Fig. 15. The perceived depth is affected by the surrounding, and so, even though bar A and bar B are at the same physical depth, they are perceived as though bar A is in front of bar B.

5 SIMULATION RESULTS

We assume that the features information is represented, and we are not concerned with the issue of how this information was acquired. This assumption is quite valid because many techniques of depth/size/curves (and therefore – their curvature) estimation are available today. An example for such technique for curves is presented by Parent & Zucker (1989) and Zucker et al (1988).

In order to simulate a feature processing and see its effect on a human observer, a tool (Matlab function) that draws image corresponding to its feature information input was created. The image was then drawn according to its original feature information, and according to its processed feature information.

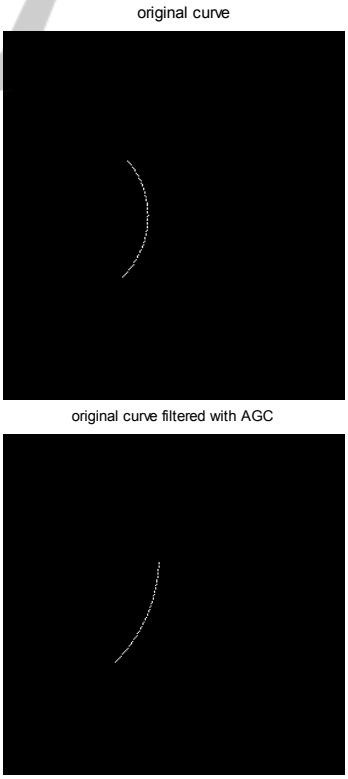

Figure 16: AGC of constant curvature.

5.1 AGC of Curvature Processing

In this section two curves are presented. The first one is a curve with constant curvature – part of a circle (Fig. 16). The second is a combination of straight lines and parts of circles with an opposite curvature (Fig. 17).

The AGC parameters for both curves are:

$$W(i) = k\frac{\gamma}{2}e^{-\gamma|i|}; k = 20; \gamma = 0.2\ , \qquad (18)$$

with W having 5 elements.

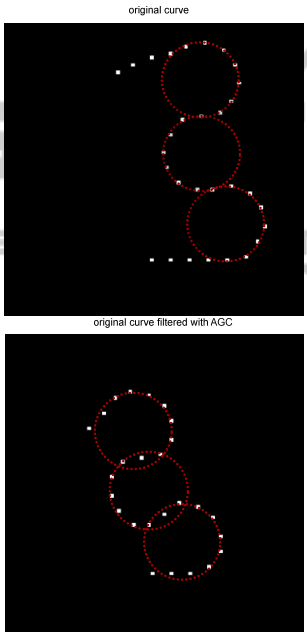

Figure 17: AGC of fragmented curvature.

The first result represents spatial adaptation – the curvature decreased (the radius of the curved increased according to (16)), whereas the second result represents curvature enhancement (or emphasis). For presentation and comparison purposes only, the result of the second curve is multiplied by 1.87, to "compensate" for the adaptation phenomenon – in order to correct comparison between the original curve and the filtered curve. Red circles have been added to Fig. 17 to emphasis the changes between the original curve, and the result. According to (16), points that are inside the circles have larger curvature than points that are on the circle. T herefore, the edge points (where a change in the curvature occurs) are emphasized in the same way as at Fig. 4.

5.2 AGC of Size Processing

The two experiments of Roberts et al. were reconstructed using Matlab and simulating the perceived target size by using the AGC algorithm presented in section 2 using parameters of:

$$W(i) = k(\frac{2}{121} - \gamma|i|)\ when: k = 5, \gamma = 0.00007\ , \qquad (19)$$

meaning that the lateral effect of W is a triangular function with width of 121 elements.

First, experiment 1 was reconstructed. Target was surrounded by 8 inducers at different radii (varying from 5 to 20 pixels). This was checked for near (30 pixels away from target), medium (40 pixels away from target) and far (50 pixels away from target) inducers. Target radius was 10 pixels. Target size (in pixels) as a function of inducer radius and distance is shown at Fig. 18.

Second, experiment 3 was reconstructed. Target was surrounded by variant number of inducers in order to occupy an approximately constant proportion (about 0.75) of the surround circumference. Inducers were kept at a constant radius and their distance from the target was changed from 30 to 60 pixels. Target radius was 10 pixels. Target size (in pixels) as a function of inducer distance is shown in Fig. 19. The solid line in this figure is the best fit for the data.

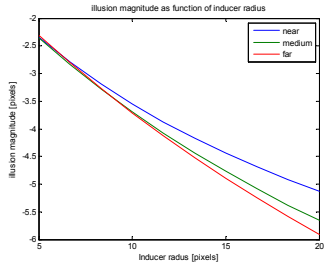

Figure 18: Results of experiment 1 using AGC model.

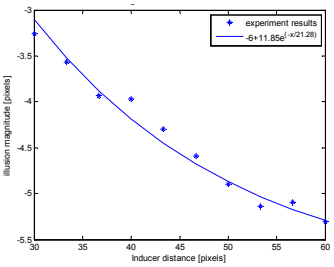

Figure 19: Results of experiment 3 using visual AGC model.

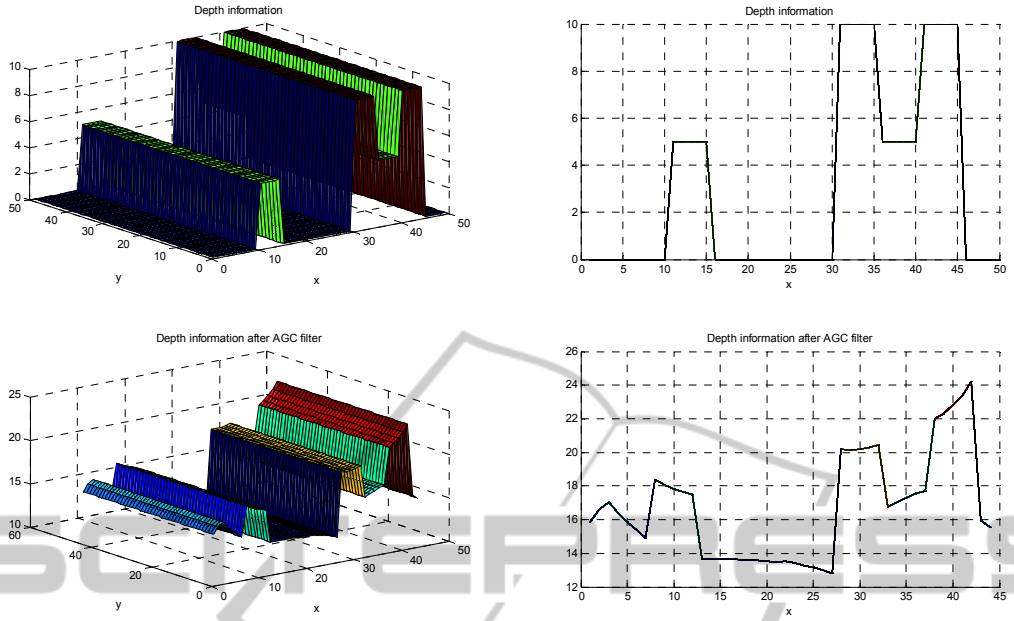

Figure 20: AGC processing of depth information. Input and output visual signals are displayed in the top and bottom rows, respectively.

5.3 AGC of Depth Processing

We reconstruct Graham and Rogers's experiment using the visual AGC NN, implemented along the visual dimension of depth, with:

$$W(i) = k\frac{\gamma}{2}e^{-\gamma|i|}; k = 1; \gamma = 0.2\,, \qquad (20)$$

where W has 11 elements.

For each point of the 3D original image the depth is calculated relative to a point in the middle of the image and with height of 50 pixels. Fig. 20 shows the results in both 3D and cross sections view. As a result of the AGC, the left bar, which is at the same depth as the right bar, is now perceived closer.

6 DISCUSSION

Qualitatively speaking, important and interesting events along curves, for example, consist only of abrupt changes of orientation and curvature, as is the case with other image attributes (dimensions). Local maxima of curvature, and inflection points (i.e. zero crossings of curvature) identify in this case such events (see (Hoffman & Richards 1984), (Koenderink & Doom 1982), (Richards et al. 1986) and (Fischler & Bolles 1986)).

Therefore, it is reasonable to assume that visual systems emphasize these changes and adapt to the locally-constant value. This is indeed an important feature of processing curvature (or other image attributes) by adaptive NN endowed with the characteristic of AGC. Curvature emphasis (as is demonstrated in Fig. 17) and adaptation (as is demonstrated in Fig. 16) occur simultaneously and their extent can be controlled by varying the parameter k of the NN hardwired connectivity. Further, the effective range of interaction, characterized in the hardwired network by $1/\gamma$, becomes, due to the AGC of the nonlinear NN a function of the slow rate of change ('local DC', i.e. C_s of Eq. 6) along the image dimension processed by the AGC NN, i.e. in the examples of Fig. 16 and Fig. 17 the curvature.

Inspecting the results of size processing indicates a good correspondence between the adaptive NN response (Fig. 18 and Fig. 19) and the psychophysical experimental results (Fig. 13 and Fig. 14), both for the distance parameter and for the size parameter. Such results should be expected due to the dependency of AGC NN on these two parameters as well, i.e. cells proximity and specificity (in this case, objects' size).

It is clear why increasing the inducer size

decreases the target perceived size. This is discussed in section 2, and represents the size contrast effect of the model. It is less obvious why farther positioned inducers have stronger effect on target perceived size, than that of the closer inducers (i.e. decreasing the target size more effectively). The latter is due to the mutual relation between the inducers. According to the model of AGC visual processing, the cells have a limited influence on their neighbors. If the distance between cells is greater compared with W's effective width, then those cells will have a minimum effect on each other (if any). When an inducer is at a given distance x from the target, its distance from the other inducers varies from 0 to $2x$. Thus, when distance increases, more and more inducers are beyond the 'influence zone' of the other inducers. This causes the perceived size of each inducer to increase when the distance is increased. Fig. 21 shows this phenomenon on the data of experiment 1. Since the target is still inside the 'influence zone' of the inducers, and the size of the inducers is now larger, the target seems smaller (the size-contrast effect is enhanced).

When we add inducers while increasing the distance (as in experiment 3), the target size is reduced since each one of the inducers contribute to the size-contrast effect.

Note that here we modelled only the target and the inducers as objects with size. But, it is also possible that the visual system treats the space between the target and the inducers as an object with size. In this case, if the space between the target and the inducer is large, the inducer size has only a secondary effect, and the target size is determined mainly by the nearest object (for example see Fig. 22 - Delboeuf illusion. In this illusion, the target gets smaller when the inducer diameter increases). This model can explain also the moon size illusion.

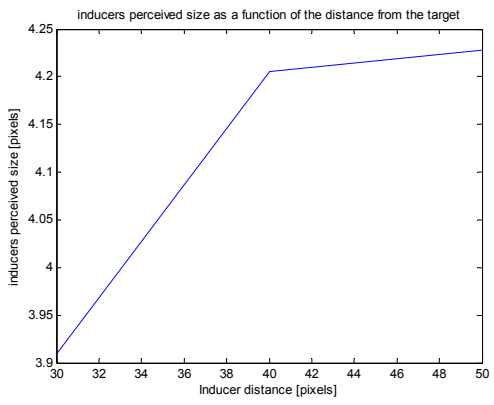

Figure 21: Results indicating that inducers perceived size is increased at greater distances.

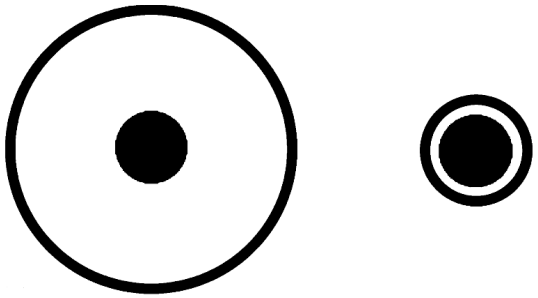

Figure 22: Delboeuf illusion.

7 CONCLUSIONS

Understanding the HVS and modelling certain characteristics of it by adaptive NN is of a considerable interest because of its potential use in the design of intelligent computer vision and image processing NN and systems. Because of the complexity of the processes involved, and in order to account for the vast volume of available experimental data, there is need for relatively simple models. As shown, the recurrent nonlinear adaptive NN that exhibits AGC is relatively simple (only few parameters) and versatile. It does not call for postulating any components of neural circuitry more complex than those well known to exist in biological neural networks. It is important to stress that these networks are sparsely connected. This fact allows also to implement them sequentially by using Peano – Hilbert scan for a quick and efficient processing 'on the fly' (for a review see (Jagadish 1990)). The sparse NN proposed by us is in contrast to Hopfield-type networks that are fully connected. The sparsely (locally) connected NN can be also analyzed theoretically (Shefer 1979).

Using the AGC model for all of the image base dimensions (or other modalities for this matter) provides great advantages. It constitutes a universal and parsimonious model that explains how our visual system processes visual information along its various dimensions, before the later stage of sequential "visual routines" is implemented. Having this model allows us to process an image not only in the intensity/spatio-temporal domain, but also along all other dimensions as well. For example, given a noisy curve, we can reduce the noise along the curvature dimension with standard filters, such as non-linear diffusion filter (Fig. 23).

The proposed visual AGC mechanism can enhance existing schemes of intelligent image processing with reference to enhancement of various image attributes and features, i.e. curvature, size and

other image attributes. The decomposition of the image into separable components is by no means the only possible model of representation and processing of images, and definitely not always the optimal one. An alternative approach, introduced in the context of image processing and computer vision (Kimmel et al. 2000), (Sochen & Zeevi 1998), considers an image to be a manifold embedded in higher dimensional combined position (spatial)-feature space. The features are the image attributes or dimensions, such as color, curvature and size mentioned above. Adaptation by means of nonlinear gain control is executed in this case in the multidimensional space in a unified manner. Such manifolds of adaptive NN are yet to be further investigated.

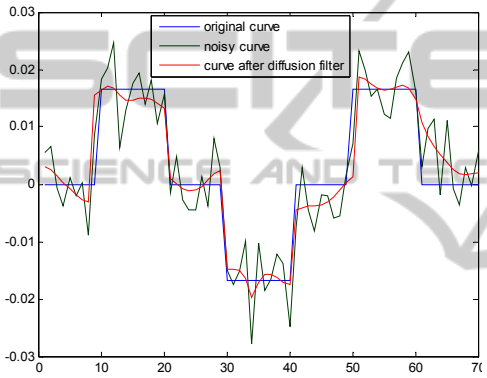

Figure 23: Filtering a noisy curve with non-linear diffusion filter (15 iterations) along the curvature dimension.

REFERENCES

Abbott, L. F. et al., 1997. Synaptic Depression and Cortical Gain Control. Science, 275(5297), 221-224.

Blakemore, C. & Campbell, F. W., 1969. On the existence of neurones in the human visual system selectively sensitive to the orientation and size of retinal images. The Journal of Physiology, 203(1), 237-260.1.

Bradshaw, M. F., Parton, A. D. & Glennerster, A., 2000. The task-dependent use of binocular disparity and motion parallax information. Vision Research, 40(27), 3725-3734.

Bradshaw, M. F. & Rogers, B. J., 1996. The Interaction of Binocular Disparity and Motion Parallax in the Computation of Depth. Vision Research, 36(21), 3457-3468.

Bruckstein, A. M. & Zeevi, Y.Y., 1979. Analysis of "integrate-to-threshold" neural coding schemes. Biological Cybernetics, 34(2), 63-79.

Bruno, N. & Cutting, J. E., 1988. Minimodularity and the perception of layout. Journal of Experimental Psychology. General, 117(2), 161-170.

Carey, D. P., Harvey, M. & Milner, A. D., 1996. Visuomotor sensitivity for shape and orientation in a patient with visual form agnosia. Neuropsychologia, 34(5), 329-337.

Cavanagh, P., Arguin, M. & Treisman, A., 1990. Effect of surface medium on visual search for orientation and size features. Journal of Experimental Psychology: Human Perception and Performance, 16(3), 479-491.

Coltheart, M., 1971. Visual feature-analyzers and aftereffects of tilt and curvature. Psychological Review, 78(2), 114-121.

Dijkstra, T. M. H. et al., 1995. Perception of three-dimensional shape from ego- and object-motion: Comparison between small- and large-field stimuli. Vision Research, 35(4), 453-462.

Ding, J. & Sperling, G., 2006. A gain-control theory of binocular combination. Proceedings of the National Academy of Sciences of the United States of America, 103(4), 1141-1146.

Dobbins, A., Zucker, S.W. & Cynader, M. S., 1987. Endstopped neurons in the visual cortex as a substrate for calculating curvature. Nature, 329, 438-441.

Du Croz, J. J. & Rushton, W. A. H., 1966. The separation of cone mechanisms in dark adaptation. The Journal of Physiology, 183(2), 481-496.

Enns, J. T. & Rensink, R. A., 1990a. Influence of scene-based properties on visual search. Science (New York, N.Y.), 247(4943), 721-723.

Enns, J. T. & Rensink, R. A., 1990b. Sensitivity to Three-Dimensional Orientation in Visual Search. Psychological Science, 1(5), 323-326.

Fischler, M. A. & Bolles, R. C., 1986. Perceptual organization and curve partitioning. IEEE Trans. Pattern Anal. Mach. Intell., 8(1), 100-105.

Gibson, J.J., 1937. Adaptation with negative after-effect. Psychological Review, 44(3), 222-244.

Ginosar, R., Hilsenrath, O. & Zeevi, Y. Y., 1992. United States Patent: 5144442 - Wide dynamic range camera.

Graham, M. & Rogers, B. J., 1982. Simultaneous and successive contrast effects in the perception of depth from motion-parallax and stereoscopic information. Perception, 11(3), 247 – 262.

Hancock, S. & Peirce, J. W., 2008. Selective mechanisms for simple contours revealed by compound adaptation. Journal of Vision, 8(7), 1-10.

Hochstein, S. & Ahissar, M., 2002. View from the top: hierarchies and reverse hierarchies in the visual system. Neuron, 36(5), 791-804.

Hoffman, D. D. & Richards, W.A., 1984. Parts of recognition. Cognition, 18(1-3), 65-96.

Hubel, D. H. & Wiesel, T. N., 1979. Brain mechanisms of vision. Scientific American, 241(3), 150-162.

Hubel, D. H. & Wiesel, T. N., 1968. Receptive fields and functional architecture of monkey striate cortex. The Journal of Physiology, 195(1), 215-243.

Hubel, D. H. & Wiesel, T. N., 1962. Receptive fields, binocular interaction and functional architecture in the cat's visual cortex. Journal of Physiology (London), 160(1), 106-154.

Hubel, D. H. & Wiesel, T. N., 1970. Stereoscopic Vision in Macaque Monkey: Cells sensitive to Binocular Depth in Area 18 of the Macaque Monkey Cortex. Nature, 225, 41-42.

Inui, T. et al., 2000. Neural substrates for depth perception of the Necker cube; a functional magnetic resonance imaging study in human subjects. Neuroscience Letters, 282(3), 145-148.

Jagadish, H. V., 1990. Linear clustering of objects with multiple attributes. In Proceedings of the 1990 ACM SIGMOD international conference on Management of data, 332-342.

Kimmel, R., Malladi, R. & Sochen, N., 2000. Images as Embedded Maps and Minimal Surfaces: Movies, Color, Texture, and Volumetric Medical Images. International Journal of Computer Vision, 39(2), 111-129.

Koenderink, J. J. & Doom, A. J .V., 1982. The shape of smooth objects and the way contours end. Perception, 11(2), 129 – 137.

Koenderink, J. J. & Doorn, A. J. V., 1987. Representation of local geometry in the visual system. Biological Cybernetics, 55(6), 367-375.

Krauskopf, J. & Mollon, J. D., 1971. The independence of the temporal integration properties of individual chromatic mechanisms in the human eye. The Journal of Physiology, 219(3), 611-623.

Lu, Z. & Sperling, G., 1996. Contrast gain control in first- and second-order motion perception. Journal of the Optical Society of America A, 13(12), 2305-2318.

Parent, P. & Zucker, S.W., 1989. Trace Inference, Curvature Consistency, and Curve Detection. IEEE Transactions on Pattern Analysis and Machine Intelligence, 11(8), 823-839.

Ratliff, F., 1965. Mach bands: Quantitative studies on neural networks in the retina. Holden-Day inc.

Richards, W., Dawson, B. & Whittington, D., 1986. Encoding contour shape by curvature extrema. Journal of the Optical Society of America A, 3(9), 1483-1491.

Riggs, L. A., 1973. Curvature as a Feature of Pattern Vision. Science, 181(4104), 1070-1072.

Roberts, B., Harris, M.G. & Yates, T.A., 2005. The roles of inducer size and distance in the Ebbinghaus illusion (Titchener circles). Perception, 34(7), 847 – 856.

Rogers, B. J. & Graham, M., 1979. Motion parallax as an independent cue for depth perception. Perception, 8(2), 125 – 134.

Schwartz, O. & Simoncelli, E. P., 2001. Natural signal statistics and sensory gain control. Nat Neurosci, 4(8), 819-825.

Shefer, M., 1979. AGC models for retinal signal processing. M.Sc. Thesis. Technion.

Sochen, N. & Zeevi, Y. Y., 1998. images as manifolds embedded in a spatial feature non euclidean space. IEEE ICIP, 166-170.

Stromeyer, C. F. & Riggs, L.A., 1974. Curvature Detectors in Human Vision? Science, 184(4142), 1199-1201.

Sutherland, N. S., 1968. Outlines of a Theory of Visual Pattern Recognition in Animals and Man. Proceedings of the Royal Society of London. Series B, Biological Sciences, 171(1024), 297-317.

Treisman, A. M. & Gormican, S., 1988. Feature analysis in early vision: Evidence from search asymmetries. Psychological Review, 95(1), 15-48.

Wainwright, M. J., 1999. Visual adaptation as optimal information transmission. Vision Research, 39(23), 3960-3974.

Weltsch-Cohen, Y., 2002. AGC models for signal processing in the primary visual cortex. M.Sc. Thesis. Technion.

Wolfe, J. M. et al., 2003. Changing your mind: On the contributions of top-down and bottom-up guidance in visual search for feature singletons. Journal of Experimental Psychology: Human Perception and Performance, 29(2), 483-502.

Zeevi, Y. Y., Ginosar, R. & Hilsenrath, O., 1995. United States Patent: 5420637 - Dynamic image representation system.

Zeevi, Y. Y. & Kronauer, E. R., 1985. Reorganization and diversification of signals in vision. EEE transactions on systems, man, and cybernetics, 15(1), 91-101.

Zeevi, Y. Y. & Mangoubi, S.S., 1978. Noise suppression in photoreceptors and its relevance to incremental intensity thresholds. Journal of the Optical Society of America, 68 (12), 1772-1776.

Zucker, S. W. et al., 1988. The Organization Of Curve Detection: Coarse Tangent Fields And Fine Spline Coverings. In Computer Vision., Second International Conference, 568-577.